Macromolecules

pubs.acs.org/Macromolecules Article

Ultrastructure of Critical-Gel-like Polyzwitterion–Polyoxometalate Complex Coacervates: Effects of Temperature, Salt Concentration, and Shear

Benxin Jing, Manuela Ferreira, Kehua Lin, Ruipeng Li, Benjamin M. Yavitt, Jie Qiu, Masafumi Fukuto, and Yingxi Zhu*

Cite This: *Macromolecules* 2020, 53, 10972–10980 Read Online

ABSTRACT: The structure of unconventional complex coacervates, such as polymer–nonpolymer complex coacervates, remains less investigated than that of the conventional coacervates formed between oppositely charged polyelectrolytes with symmetric charge species. Yet, their microscopic structural organization is important to further elucidate the mechanism of liquid–liquid-phase separation processes upon complexation. In this work, we characterize the microstructural organization of complex coacervates formed between inorganic polyoxometalate (POM) and polyzwitterion by small-angle X-ray scattering (SAXS) with in situ temperature and shear control. Despite the apparent transparent and homogeneous morphology of dense coacervates as observed by optical microscopy, our previous results (*Macromolecules* **2018**, *51*, 22, 9405–9411) suggest that dense polyzwitterion–POM coacervates exhibit critical-gel-like networks containing both complex-poor region (mesh pore) and complex-rich region (connective network). SAXS results as reported in this work support that the complex-rich region is actually in the form of loosely packed POM aggregates linked by polyzwitterion, designated as complex particles. The structure of aggregating complex particles is further examined against varied composition and salt concentrations, temperature, and shear, thanks to the high X-ray scattering contrast of POMs from that of other components in the coacervates. The complex particles in the dense coacervates appear to grow with more tightly packed POM aggregates with increasing POM-to-polyzwitterion concentration ratio, in contrast to more loosely packed POM aggregates with decreasing salt concentration. Conversely, increasing temperature could result in smaller complex particles containing more loosely packed POM aggregates, consistent with temperature-dependent viscoelasticity of dense coacervates. Furthermore, such POM-based hybrid dense coacervates exhibit intriguing strain-hardening behavior, resulting from shear-enhanced POM packing inside the complex particles. Distinct from the shear-thinning behavior of most conventional cross-linked polymeric networks, the strain-hardening property combined with thermal- and salt-responsive characteristics of polyzwitterion–POM coacervates could broaden the applications of hybrid organic–inorganic macroion coacervates as smart functional materials working under extreme environmental conditions.

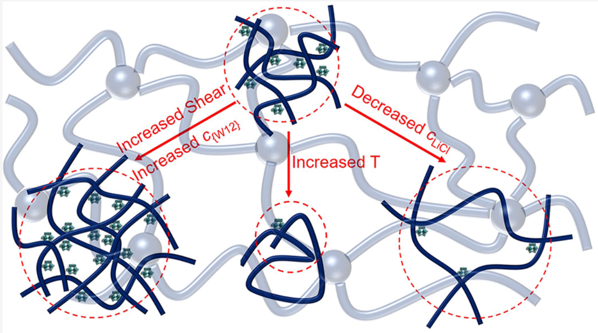

PSBMA-$\{W_{12}\}$ complex particles in critical-gel-like dense coacervate

INTRODUCTION

Since the Dutch Chemist, Prof. H.G. Bungenberg de Jong introduced the concept of "coacervation" in 1929,[1] a wide variety of complex coacervates have been discovered in nature and reproduced synthetically in labs.[2−4] Complex coacervates exhibit many intriguing physical properties such as unique liquid-phase stability,[5,6] ultralow interfacial tension,[7−9] and widely tunable mechanical properties,[10,11] leading to their wide applications on drug/gene delivery,[12] tissue culture scaffolds,[13] underwater adhesives,[14,15] and membrane-less organelles.[16−19] In the past decade, complex coacervates have thereby attracted emerging scientific interest in fundamentally understanding their thermodynamic origin,[5,6,20] phase behavior,[5,6,21−24] and microscopic structural organization.[25−27] Polyelectrolyte complex coacervates, which are formed between oppositely charged flexible polyelectrolytes with symmetric charge sites in salted water, have been most widely investigated as model synthetic coacervate systems.[28] Recently, other polymeric macroions, semiflexible and even nonflexible macroions such as folded proteins,[29−31] surfactant micelles,[32,33] dendrimers,[34] and inorganic polyoxometalates,[35−39] are also introduced to enrich

Received: July 14, 2020
Revised: October 20, 2020
Published: December 8, 2020

https://dx.doi.org/10.1021/acs.macromol.0c01618
Macromolecules 2020, 53, 10972−10980

the coacervate family with broadened material properties and emerging new applications.

The properties and performance of functional complex materials can be greatly governed by their structures. The introduction of semiflexible and nonflexible macroions to the family of complex coacervates could complicate the matter because of their distinct molecular geometry and surface-charge patterning.[28] Yet, it is critical and imperative to reveal the structural organization of unconventional coacervates at micro- and nanoscale so as to further elucidate the mechanisms of general liquid−liquid-phase separation processes upon complexation.[25−27] Despite great efforts on disclosing the structure of complex coacervates by different experimental techniques such as small-angle scattering (including light scattering (SALS), X-ray scattering (SAXS), and neutron scattering (SANS)),[25,40−44] cryo-TEM and liquid TEM,[26,27,45−47] and fluorescence techniques,[9,37] the ultrastructure, which is a fine structure at nanoscales, of coacervates remains debated. Presently, two distinct ultrastructural models have been proposed and debated for conventional polyelectrolyte coacervates as well as some other coacervates containing proteins and surfactant micelles: interpenetrated overlapping or semidilute polymer solution[44,48] and bifluidic sponge-like nanostructured network.[9] It is noted that small-angle scattering experiments, especially SAXS and SANS with high spatial resolution at the sub-nanometer level, could offer much more detailed structural information than TEM. However, the inherent inhomogeneity of polymers, arising from the polydispersity in molecular weight, randomness in monomer sequence, and variable chain conformations, makes it difficult to perform straightforward structural analysis of scattering data without model dependence. Hence, a new coacervate system built with homogeneous components could be highly desired to explore the ultrastructure of complex coacervates by scattering techniques.

In our recent work, we have successfully introduced a family of giant molecules of transition-metal oxide, polyoxometalates (POMs) of 0.8−6 nm in diameter and bearing negative charges in aqueous solutions to form liquid−liquid separating coacervates with sulfobetaine-based zwitterionic polymers.[37,38] As POMs have been explored as novel functional nanomaterials used for catalysis,[49,50] semiconductors,[51] anticancer/virus, and antiamyloid treatments,[52,53] introducing POMs to coacervate materials would greatly broaden the applications of complex coacervates with significant enhancement of their mechanical strength. For the coacervation between zwitterionic polysulfobetaine and anionic POM in salted aqueous solutions, we have confirmed that the enthalpy change upon their coacervation is negligible based on isothermal titration calorimetric measurements. The composition analysis has confirmed that the salt concentration in supernatant is higher than that in dense coacervates, while polymer and POM concentrations in dense coacervates are higher than those in supernatant,[37,54] consistent with the polymer-poor supernatant and polymer-rich coacervate phase of common polyelectrolyte coacervates. Thus, we have clearly demonstrated that hybrid polyzwitterion−POM coacervates are indeed entropy-driven liquid−liquid-separating complexes similar to those biological and synthetic polyelectrolyte coacervates.[37,38] However, the entropy gain upon polyzwitterion−POM coacervation results from the release of monovalent anions that are bound with polyzwitterions and replaced by multivalent anionic POMs to form polyzwitterion−POM links, different from the release of the counterions near polycations and polyanions upon coacervation of conventional polyelectrolytes. Accordingly, we have observed that polyzwitterion−POM complex coacervates exhibit some distinct features from conventional polyelectrolyte coacervates, including salt-broadened coacervate phase due to "anti-polyelectrolyte" behavior of polyzwitterion and strong thermo- and salt-stimuli responses.[55−57] Most strikingly, we have observed a critical-gel-like behavior of polyzwitterion−POM dense coacervates, where elastic and viscous shear moduli overlap over a wide range of shear frequency, temperature, and salt concentration without a well-defined gel point,[37] in sharp contrast to the liquid-like behavior with a terminal relaxation time of conventional polyelectrolyte coacervates.[58] The critical-gel-like behavior suggests a self-similar percolative network structure of polyzwitterion−POM dense coacervates, distinct from the interpenetrated overlapping polymer solution behaviors as previously reported for conventional polyelectrolyte coacervates.[44,48] Hence, direct experimental characterization to reveal the ultrastructure of polyzwitterion−POM dense coacervates in relation to their critical-gel-like behavior is imperatively demanded.

We have previously employed fluorescence recovery after photobleaching (FRAP) to examine the averaged mesh pore size of polyzwitterion−POM coacervate network using inert fluorescent nanoprobes of varied size.[37] The average mesh size is found to be smaller than 10 nm but much greater than the diameter (=0.8 nm) of POM, similar to the bifluidic network structure.[9] However, FRAP results could only indirectly indicate the local structural information in the *complex-poor (mesh pore)* region in dense coacervate but give little structural information of the *complex-rich (connective network)* region. In this work, we employ SAXS to further explore the ultrastructure of dense coacervates at a length scale of one to tens of nanometers. Thanks to their well-defined and stable architecture and uniform size independent of solution conditions, POMs can work as perfect model nanomaterials for small-angle scattering techniques. The electron density of transition metals of POMs is also much higher than that of the lighter elements in organic polymers (mainly hydrogen, carbon, oxygen, and nitrogen atoms).[59] Hence, POMs are ideal X-ray scattering "probes" to detect the ultrastructure of emerging complex coacervates by SAXS, similar to the isotope probes used for SANS.

Specifically, we have carried out the SAXS study of polyzwitterion−POM dense coacervates with in situ control of temperature and applied shear in this work. The POM selected in this work is lithium metatungstate, $\{W_{12}\}$ ($Li_6H_2W_{12}O_{40}$), of 0.8 nm in diameter and bearing 8 negative charges in aqueous solution. The polyzwitterion selected in this work is poly(sulfobetaine methacrylamide) (PSBMA) of molecular weight (M_w) around 5.6×10^6 g/mol and bearing zero net charge.[38] Although the radius of gyration, R_g, of PSBMA is tens of nanometers and much larger than that of $\{W_{12}\}$, the PSBMA polymer is nearly transparent to X-ray in aqueous solution due to its lighter element compositions and highly swollen state. With in situ temperature and shear control during SAXS measurements, we have systematically examined the effects of composition concentration, temperature, and shear strain on the structural change of PSBMA−$\{W_{12}\}$ complex-rich region in the critical-gel-like dense coacervates.

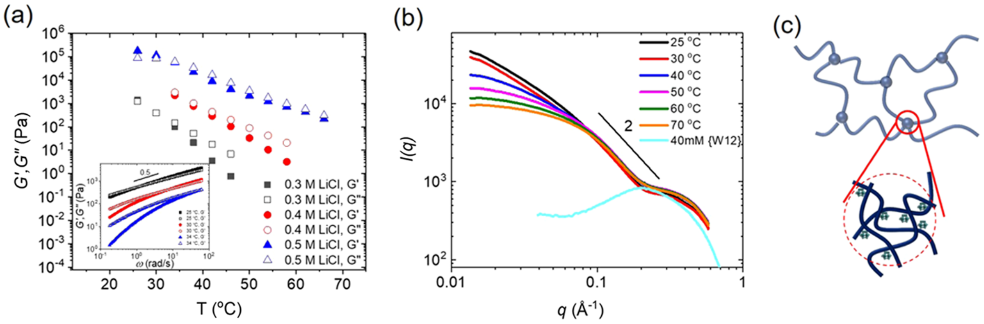

Figure 1. (a) Temperature-dependent shear moduli of G' (elastic moduli, solid symbols) and G'' (viscous moduli, open symbols) of PSBMA−$\{W_{12}\}$ dense coacervates formed at fixed $c_{SBMA} = 25$ g/L and $c_{e\{W12\}}/c_{SBMA} = 160\%$ but varied c_{LiCl}. Linear viscoelasticity of the dense coacervates was acquired at a constant angular frequency, $\omega = 6.28$ rad/s, and shear strain $\gamma = 1\%$. Inset: ω-dependent linear viscoelastic spectra of PSBMA−$\{W_{12}\}$ dense coacervates formed at fixed $c_{SBMA} = 25$ g/L, $c_{e\{W12\}}/c_{SBMA} = 160\%$, and $c_{LiCl} = 0.3$ M, acquired at $\gamma = 1\%$ and varied $T = 26$ °C (black squares), 30 °C (red circles), and 34 °C (blue triangles). (b) T-dependent SAXS intensity, $I(q)$, of PSBMA−$\{W_{12}\}$ dense coacervates (at rest) formed at fixed $c_{SBMA} = 25$ g/L, $c_{e\{W12\}}/c_{SBMA} = 160\%$, and $c_{LiCl} = 0.3$ M, after normalization by their transmission ratio and subsequent subtraction of the background intensity of deionized water. $I(q)$ of PSBMA−$\{W_{12}\}$ dense coacervates is in sharp contrast to that of PSBMA-free $\{W_{12}\}$ of 40 mM in PSBMA-free dilution aqueous solution (cyan solid line). (c) Schematic illustration of *complex particles* in the connective network of PSBMA−$\{W_{12}\}$ dense coacervates.

■ EXPERIMENTAL SECTION

PSBMA was synthesized from [3-(methacryloylamino)propyl]-dimethyl(3-sulfopropyl)ammonium hydroxide inner salt (Monomer Polymer & Dajac Labs) by strictly following a published procedure.[38] Aqueous solution of lithium metatungstate, $\{W_{12}\}$ ($Li_6H_2W_{12}O_{40}$), was purchased from LMT Liquid and freeze-dried (Labconco Freezone 4.5 Freeze-Dryer) before experiments.

Dense PSBMA−$\{W_{12}\}$ coacervates were prepared by strictly following our previously published procedure.[37] Briefly, biphasic coacervate complexes were centrifuged (Sorvall Legend X1R Centrifuge, Thermo Scientific) at 22 800*g* and 22 °C for at least 12 h to thoroughly remove the dilute supernatant phase from the dense coacervate phase. It is noted that no effect of centrifugal acceleration on the structure and rheological properties of dense coacervate was observed. The absence of the supernatant phase was verified by featureless morphology of dense coacervates with added fluorescence-labeled PSBMA by super-resolution confocal laser scanning microscopy (CLSM, Carl Zeiss LSM 780) with a 63× objective lens (Plan-Apochromat, NA = 1.4, oil immersion) and an Airyscan detector (Carl Zeiss). In this work, the total concentration of PSBMA in the complex coacervates was kept constant based on its monomer concentration, $c_{SBMA} = 25$ g/L, while the $\{W_{12}\}$ concentration, $c_{\{W12\}}$, and LiCl concentration, c_{LiCl}, were varied to tune the microstructure and rheological properties of PSBMA−$\{W_{12}\}$ dense coacervates.

The linear viscoelasticity of PSBMA−$\{W_{12}\}$ dense coacervates was measured on a stress-controlled rheometer (Malvern Bohlin Gemni HRnano) with the parallel-plate fluid cell of 20 mm in diameter and 1000 μm in gap spacing at fixed shear strain, $\gamma = 1\%$, and varied applied oscillatory shear frequency, ω. Nonlinear oscillatory shear spectra in response to varied $\gamma = 0.1$−3000% were obtained at constant $\omega = 6.28$ rad/s. To prevent the slip of samples during shear, sandpaper of grit size 600 (47185A51, McMaster-Carr) was glued to the surfaces of a parallel-plate fluid cell used for rheology measurements. After sample loading and the desired gap spacing between the parallel plates were achieved, a thin film of paraffin oil (Aldrich) was applied to seal the edge of the sample to minimize the evaporation of water in samples. Temperature was varied from 2 to 70 °C using a Peltier Element equipped with the rheometer. For each temperature, the sample was equilibrated for 10 min to ensure proper thermal and sample stability before measurements.

The ultrastructure of dense PSBMA−$\{W_{12}\}$ coacervates was characterized by SAXS equipped with an optical shearing cell (CSS450, Linkam Scientific) at the Complex Materials Scattering (CMS/11-BM) beamline of the National Synchrotron Light Source II (NSLS-II), Brookhaven National Laboratory (BNL). SAXS experiments were carried out with the incident X-ray wavelength, $\lambda = 0.0729$ nm (X-ray energy of 17 keV to lower the absorption of X-ray by W atoms), using a Pilatus 2M detector (Dectris, Baden-Dättwil, Switzerland). For static SAXS experiments, the coacervate samples were loaded into quartz capillary tubes (Charles-Supper) of 1.5 mm in diameter. The distance between the coacervate sample and the SAXS detectors was 2.0 m. For in situ SAXS experiments under oscillatory shear at 30 °C similar to the rheology measurements as reported in this work, the samples were loaded into the optical shearing cell backed with Kapton windows at a gap of 1.0 mm and equilibrated for 30 min before SAXS measurement, for which the distance between the sample and the SAXS detectors was set fixed at 5.85 m. The wide-angle scattering intensity (WAXS) was collected on a Pilatus 300K detector (Dectris, Baden-Dättwil, Switzerland), with the detector distance set at 160 mm away from the sample, to complement SAXS results. For SAXS experiments with or without shear, the distance between samples and SAXS detectors was calibrated using silver behenate with the first-order reflection at a scattering vector of $q = 1.076$ nm^{-1}, where $q = (4\pi \sin\theta)/\lambda$ with θ being the half-scattering angle. For temperature-dependent SAXS measurements, the temperature was varied from 25 to 70 °C with an accuracy of ±0.1 °C, and at each temperature, a waiting time of 30 min was applied before SAXS measurements to ensure thermal equilibrium of coacervate samples. Due to a much longer waiting time for cooling with the optical shearing cell, we were unable to repeat the SAXS measurements with decreasing temperature. Data acquisition time for each SAXS exposure was 30 s. All of the SAXS intensity profiles of dense coacervates were first normalized by their transmission ratio and subsequently subtracted by the transmission-corrected SAXS profile of deionized water to produce background-corrected and subtracted SAXS profiles for further data analysis.

■ RESULTS AND DISCUSSION

PSBMA−$\{W_{12}\}$ complex coacervates exhibit unique critical-gel-like dynamic structure as detailed in our recently reported rheological study.[37] The linear viscoelastic results for dense PSBMA−$\{W_{12}\}$ coacervates of constant $c_{e\{W12\}}/c_{SBMA} = 160\%$, which is the ratio of 8 × $\{W_{12}\}$ molar concentration to PSBMA monomer concentration, c_{SBMA} (=25 g/L), at varied LiCl concentration, $c_{LiCl} = 0.3$, 0.4, and 0.5 M, are shown in Figure 1a. The elastic modulus, G', of dense coacervates nearly overlaps with the viscous modulus, G'', over a wide range of temperature, suggesting a pronounced critical-gel-like structure that behaves between liquid-like solution and solid-like gel.[60,61] It is noted that such viscoelastic behavior is reversible without apparent hysteresis upon complete temperature sweep. In

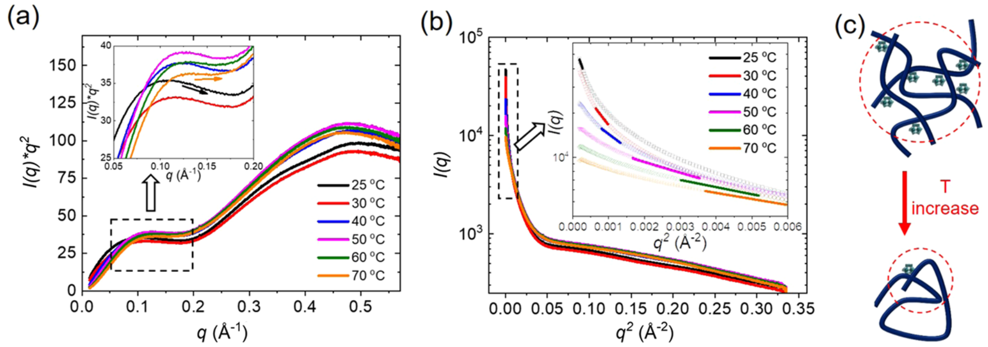

Figure 2. (a) Kratky plots of $I(q) \times q^2$ against q and (b) Guinier plots of $I(q)$ against q^2 of PSBMA−{W$_{12}$} dense coacervates formed at fixed c_{SBMA} = 25 g/L, $c_{\mathrm{e\{W12\}}}/c_{\mathrm{SBMA}}$ = 160%, and c_{LiCl} = 0.3 M but varied temperature. The inset in (a) corresponding to the dashed box is the "zoom-in" tails directed by the arrows. The inset in (b) corresponding to the dashed box is the "zoom-in" corresponding to q^2 from 0 to 0.006 Å^{-2}, where the colored lines correspond to the best-fit in the Guinier regions as determined by the GPA (see the text for details). (c) Schematic illustration of the structural change of complex particles against temperature.

frequency-dependent linear viscoelastic spectra, both G' and G'' of critical-gel-like dense coacervates scale with angular frequency, ω, in a power law as $G' \approx G'' \propto \omega^n$, where n is the viscoelastic exponent and a function of space dimension, d (=3 for our three-dimensional case), and fractal dimension, d_f, of critical gel.[62] For PSBMA−{W$_{12}$} dense coacervates, we have confirmed in our recent report that $n \sim 0.5$,[37] independent of c_{SBMA}, $c_{\mathrm{e\{W12\}}}/c_{\mathrm{SBMA}}$, and LiCl concentration, c_{LiCl}, strongly suggesting a fully screened excluded-volume effect in this system.[62] According to the relationship of d_f−dependent n developed for polymeric network with fully screened excluded-volume effect,[62] $n = \frac{d(d+2-2d_f)}{2(d+2-d_f)}$, the d_f of PSBMA−{W$_{12}$} dense coacervate is calculated to be d_f = 2. The static SAXS results as reported below further verify the fractal structure and d_f of critical-gel-like dense coacervates. As shown in Figure 1b and Supporting Figures S1 and S2, all of the SAXS intensity, $I(q)$ profiles, after background subtraction, overlap at $q > 0.1$ Å^{-1} for PSBMA−{W$_{12}$} dense coacervates of varied c_{SBMA}, $c_{\mathrm{e\{W12\}}}/c_{\mathrm{SBMA}}$, and c_{LiCl}. The power law slopes of $I(q)$ profiles against q are measured to be ∼−2.0 at 0.2 Å^{-1} > q > 0.1 Å^{-1}, strongly suggesting a fractal dimension of d_f = 2 in good agreement with measured linear frequency-dependent viscoelastic spectra.[37]

Furthermore, as shown in Figure 1b, the measured $I(q)$ of all PSBMA−{W$_{12}$} dense coacervate samples at rest increases with decreasing q at a low q region ($q < 0.2$ Å^{-1}), in sharp contrast to the opposite trend of the measured $I(q)$ of PSBMA-free {W$_{12}$} aqueous solution of similar {W$_{12}$} concentration in the same q range. The distinct intensity profiles with much enhanced scattering intensity at low q indicate the presence of {W$_{12}$}-containing complex particles in dense coacervates, with much larger size than individual {W$_{12}$} of 8 Å in diameter. It should be noted that the scattering intensity of PSBMA−{W$_{12}$} coacervates mainly results from the high electron density contrast of {W$_{12}$} from that of PSBMA, as evident from the fact that the intensity of {W$_{12}$}-free PSBMA solution is almost the same as that of deionized water as the background. The decreased intensity of PSBMA-free {W$_{12}$} aqueous solution at a low q region ($q < 0.2$ Å^{-1}) indicates the strong repulsion among highly charged {W$_{12}$},[63] excluding the possibility of {W$_{12}$} self-aggregation as the origin for the enhanced scattering intensity of the dense coacervates in Figure 1b. Hence, the {W$_{12}$}-containing particles in the dense coacervates must be the aggregates of {W$_{12}$} linked with PSBMA, designated as *complex particles* as schematically illustrated in Figure 1c.

To examine the packing of {W$_{12}$} inside the complex particles, we perform the Kratky analysis, which is often used to qualitatively examine the internal compactness of polymers and proteins or assess the degree of flexibility within the scattering particle.[64,65] For instance, an increase in $I(q)q^2$ to a plateau at high q region suggests random coil or unfolded protein, or flexible scattering particle. A bell-shaped peak suggests globule or folded protein or rigid scattering particle, while a broad peak with a nonzero tail suggests partially unfolded protein or semiflexible scattering particle. In this work, as the scattering signal of dense coacervates mainly comes from {W$_{12}$}, the internal compactness of complex particles extracted from the Kratky plots actually reflects the packing degree of {W$_{12}$} inside the complex particles. As the Kratky plots of $I(q)q^2$ against q are shown in Figure 2a and Supporting Figures S3 and S4,[64] two distinct peaks are observed, one corresponding to $q \sim 0.1$ Å^{-1} and the other corresponding to $q \sim 0.45$ Å^{-1}. The sharp and bell-shaped peaks at $q \sim 0.45$ Å^{-1}, which are also observed as a small step in Figure 1b, appear independent of temperature and clearly correspond to single {W$_{12}$} molecules with inherent rigid crystalline structure. The length scale estimated from $2\pi/q$ (q = 0.45 Å^{-1}) is about 14 Å, larger than the diameter (=8 Å) of {W$_{12}$} and attributed to the closest separation distance between nearest neighbors of {W$_{12}$} in the coacervates. However, it is clearly distinct from strong temperature-dependent peaks observed at low q (<0.2 Å^{-1}). The broad peaks at 0.1 Å^{-1} < q < 0.2 Å^{-1} (see the inset of Figure 2a as the "zoomed-in" for the dashed region) indicate that the slope of $I(q)$−q curves in Figure 1b over the same q range slightly deviates from −2, strongly suggesting loose packing of {W$_{12}$} inside each amorphous complex particles. Furthermore, the peaks at $q \sim 0.1$ Å^{-1} shift to higher q, while the tails arise with increasing temperature, suggesting that the complex particles become smaller and {W$_{12}$} in them becomes more loosely packed at higher temperature as schematically illustrated in Figure 2a, which also explains the decrease of the scattering intensity with increasing temperature as observed in Figure 1b.

To quantify the size of complex particles in PSBMA−{W$_{12}$} dense coacervates, we have performed the Guinier analysis to estimate their radius of gyration, R_g, from the Guinier plots of $\log_{10}(I(q))$ against q^2, as shown in Figure 2b and Supporting Figures S5 and S6. It is noted that the Guinier analysis has

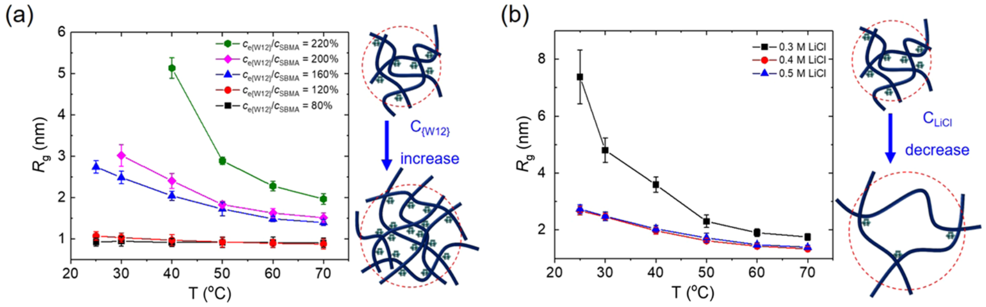

Figure 3. Effect of (a) $c_{e\{W12\}}/c_{SBMA}$ at constant c_{LiCl} = 0.5 M and (b) c_{LiCl} at constant $c_{e\{W12\}}/c_{SBMA}$ = 160% on the T-dependent gyration radius, R_g, of PSBMA−$\{W_{12}\}$ complex particles in the dense coacervates formed at fixed c_{SBMA} = 25 g/L. Next to panels (a) and (b) is the schematic illustration of the structural change of complex particles against $c_{e\{W12\}}/c_{SBMA}$ and c_{LiCl}, respectively.

been developed mainly for dilute solutions and dispersions of monodisperse particles. Thus, not all of our SAXS data measured with dense coacervates can be assumed to qualify for the Guinier analysis despite their straight-line appearance, because the excluded-volume effect could often greatly impact the analysis.[66] In this work, the excluded-volume effect could be neglected because of the fractal structure of the dense coacervates with d_f = 2 as derived from the critical-gel-like linear viscoelastic spectra and SAXS intensity profiles shown in Figure 1b. As Figures 1b and 2 clearly show no structural correlation between near-neighboring complex particles, we assume the structure factor, $S(q)$ = 1 in our case, which thereby allows us to further extract the R_g of complex particles by the Guinier analysis.

To validate the quality and valid q range of SAXS data for reliable Guinier analysis, we have employed the Guinier peak analysis (GPA) with the plot of $I(q)q$ against q^2 (see the Supporting Figures S7 and S8).[67] As shown in the Supporting Figures S7 and S8, two peaks are observed in the GPA plots, one at high q^2 ∼0.1−0.2 Å^{-2} and the other at low $q^2 \leq$ ∼0.01 Å^{-2}, verifying the validity of data quality for the Guinier analysis. It is noted that the peaks at a high q region of q^2 ∼ 0.1−0.2 Å^{-2} could be neglected as they mainly come from individual rigid $\{W_{12}\}$ corresponding to the peak at q ∼ 0.45 Å^{-1} as observed in Figure 2a and the broad linear region at q^2 > 0.05 Å^{-2} in Figure 2b. Thus, we only focus on the low q region corresponding to the peak at $q^2 \leq$ ∼0.01 Å^{-2} to evaluate the size of amorphous complex particles. With the verified presence of a peak in the GPA plots at the same q range, the Guinier plots at the low q range, where the Guinier plots appear linear against q^2 as marked in Figure 2b (colored solid lines in the inset that zooms in the dashed box region in Figure 2b), are qualified to be fitted by the following equation

$$I(q) = I_0 \exp\left(-\frac{R_g^2}{3}q^2\right) \tag{1}$$

where I_0 is the forward scattering intensity and constant,[68] yielding reliable R_g against varied solution and shear conditions.

We obtain the R_g of complex particles in PSBMA−$\{W_{12}\}$ dense coacervates corresponding to the peak at q < 0.1 Å^{-1} by fitting the Guinier plots in Figure 2b with eq 1. Accordingly, the error bars of R_g are estimated from the variance of the fitting results of 3−4 repeated measurements. As summarized in Figure 3, the R_g of complex particles calculated at q^2 < 0.01 Å^{-2} exhibits strong dependence on temperature, $c_{e\{W12\}}/c_{SBMA}$, and c_{LiCl}. At fixed $c_{e\{W12\}}/c_{SBMA}$ and c_{LiCl}, the R_g of complex particles in PSBMA−$\{W_{12}\}$ dense coacervates decreases with increasing temperature, as shown in Figure 3a. Relatedly, the shear moduli of critical-gel-like PSBMA−$\{W_{12}\}$ complex coacervates also decrease with increasing temperature, as shown in Figure 1a.[37] As the elastic modulus of the polymeric gel network is mainly governed by the polymerization degree of the network strands between cross-linking points,[69] the decrease of both complex particle size and shear moduli with increasing temperature verifies that the complex particles indeed behave like cross-linking knots for the critical-gel-like coacervate network. We recognize that such an ultrastructure of complex particles in dense coacervates is highly plausible because the chain size of the PSBMA polymer is estimated to be tens of nanometers according to its M_w ∼ 5.6 × 10^6 g/mol, much larger than the mesh pore size of dense coacervates.[37,38] Furthermore, the effect of temperature on R_g becomes even stronger with increasing $c_{e\{W12\}}/c_{SBMA}$. For instance, at $c_{e\{W12\}}/c_{SBMA}$ = 220%, R_g decreases from 5.0 to 2.0 nm as temperature increases from 40 to 70 °C, in contrast to nearly constant R_g over the same range of temperature at $c_{e\{W12\}}/c_{SBMA}$ = 80%. Combined with T-dependent linear rheology and SAXS intensity profile at low q in Figure 1 and Kratky plots in Figure 2a, the results clearly indicate that increasing temperature leads to smaller complex particles containing fewer $\{W_{12}\}$.

The effect of temperature on the structure of complex particles in PSBMA−$\{W_{12}\}$ dense coacervates can be related to T-dependent dipole interactions involving PSBMA in aqueous solution, leading to its upper critical solution temperature (UCST) behavior and thermoresponsive characteristics. Increasing solution temperature enhances the interaction between PSBMA and water but weakens the zwitterion−zwitterion interaction to improve the solubility of PSBMA in water;[56,57] conversely, the dipole−dipole interaction that essentially accounts for the zwitterion−anion binding between PSBMA and multivalent $\{W_{12}\}$, which replaces the binding between PSBMA and monovalent Cl^- anion in aqueous solution, is weakened with increasing temperature.[70] Furthermore, consistent with many reported effects of thermal fluctuations on interaction potential,[71−73] increasing temperature tends to weaken the clustering of $\{W_{12}\}$ due to its enhanced thermal fluctuation and dissociation from the complex particles. As combined, PSBMA−$\{W_{12}\}$ complex particles become smaller with a reduced number of aggregating $\{W_{12}\}$ with increasing temperature.

The R_g also increases as increasing $c_{e\{W12\}}/c_{SBMA}$ above 80%, suggesting an increased number of $\{W_{12}\}$ aggregates with PSBMA in the complex particles. It is noted that R_g ∼ 0.9 nm

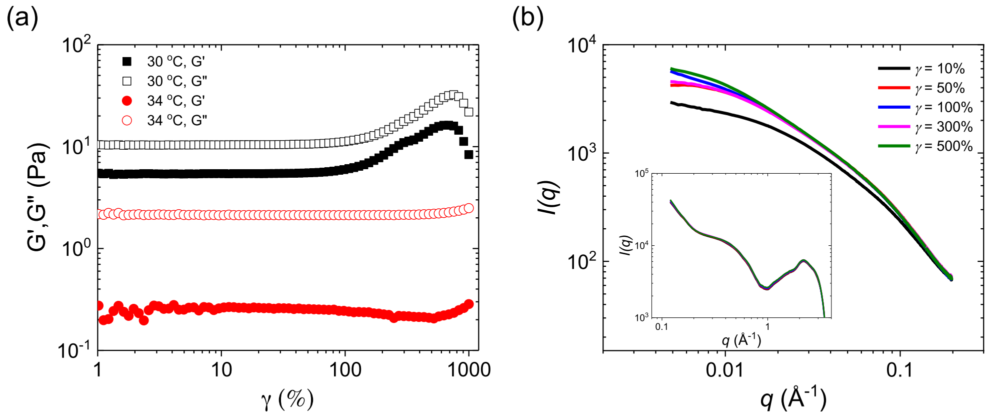

Figure 4. (a) γ-Sweep viscoelastic spectra of PSBMA−{W_{12}} dense coacervates formed at fixed c_{SBMA} = 25 g/L, $c_{e\{W12\}}/c_{SBMA}$ = 160%, and c_{LiCl} = 0.3 M measured at constant ω = 6.28 rad/s but varied T. (b) SAXS intensity, $I(q)$, for the same samples as shown in (a) acquired in situ under an applied shear of constant ω = 6.28 rad/s and T = 30 °C but varied γ. $I(q)$ was plotted after being normalized by their transmission ratio and subsequently subtraction of the background intensity of deionized water. Inset: WAXS intensity of the same samples under the same condition.

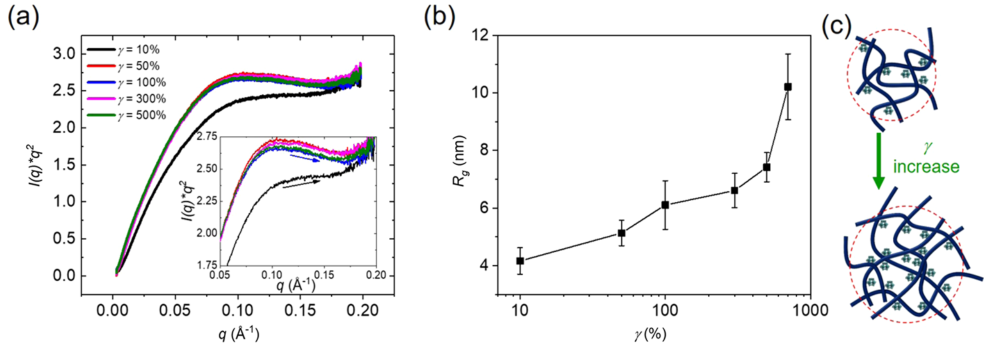

Figure 5. (a) Kratky plots of $I(q) \times q^2$ against q of PSBMA−{W_{12}} dense coacervates formed at fixed c_{SBMA} = 25 g/L, $c_{e\{W12\}}/c_{SBMA}$ = 160%, and c_{LiCl} = 0.3 M and T = 30 °C in response to applied shear of varied γ at constant ω = 6.28 rad/s. The inset is the "zoom-in" tails as directed by the arrows. (b) γ-dependent R_g of complex particles in PSBMA−{W_{12}} dense coacervates formed at the same conditions in (a). (c) Schematic illustration of the structural change of complex particles against γ.

at $c_{e\{W12\}}/c_{SBMA}$ = 80% is approximately 2.25 times as large as the radius of a single {W_{12}}, but the rising tails at $q > 0.1 Å^{-1}$ on the Kratky plots (see Supporting Figure S3) suggest that the complex particles are indeed coil-like and similar to those formed at high temperature, not the clusters of rigid {W_{12}} without PSBMA. Thus, the complex particles formed at $c_{e\{W12\}}/c_{SBMA}$ = 80% could be considered as the smallest aggregates upon PSBMA−{W_{12}} complexation. Moreover, the Kratky plots in Figure S3 indicate that the {W_{12}} complex particles become more tightly packed with increasing $c_{e\{W12\}}/c_{SBMA}$. Consequently, the observed increase of R_g for complex particles with more tightly packed {W_{12}} could result from enhanced cross-linking of PSBMA by {W_{12}} with increasing $c_{e\{W12\}}/c_{SBMA}$, as schematically illustrated in Figure 3a. Furthermore, the R_g of PSBMA−{W_{12}} complex particles also exhibits strong dependence on salt concentration, as shown in Figure 3b. At constant $c_{e\{W12\}}/c_{SBMA}$ = 160%, the complex particles formed at c_{LiCl} = 0.3 M appear to be significantly larger than those formed at c_{LiCl} = 0.4 and 0.5 M.[38] For anionic {W_{12}}, as lowering salt concentration could enhance electrostatic repulsion between {W_{12}} molecules, {W_{12}} could become more loosely packed inside complex particles, resulting in the increased R_g of complex particles at lower salt concentration, as schematically illustrated in Figure 3b.

In addition to examining the static ultrastructure of PSBMA−{W_{12}} dense coacervates, we have also investigated the effect of shear on the ultrastructure of PSBMA−{W_{12}} dense coacervates by both nonlinear oscillatory shear rheology and in situ SAXS with shear. The nonlinear rheological behavior of PSBMA−{W_{12}} dense coacervates at fixed ω = 6.28 rad/s, $c_{e\{W12\}}/c_{SBMA}$ = 160%, and c_{LiCl} = 0.3 M against shear strain amplitude, γ, is shown in Figure 4a. Critical shear strain, γ_c, at which a transition from linear to nonlinear response to applied shear occurs, can be determined from the onset shear strain where measured shear moduli commence to arise from the γ-independent plateau regime of measured G' and G'' in Figure 4a. Clearly, when γ is below a critical shear strain, γ_c, both G' and G'' of dense coacervates are nearly constant with γ, suggesting linear viscoelasticity and predominately viscous response to applied shear. At $\gamma > \gamma_c$, we observe surprisingly that both G' and G'' increase with increasing γ, exhibiting strain hardening in response to increased shear deformation. As further increasing γ to exceed the yielding point, typical shear thinning is observed, suggesting large shear deformation-induced disruption of network. γ_c is found to shift from ~50 to ~300% with increasing temperature from 30 to 34 °C, respectively. More importantly, the strain-hardening characteristics of PSBMA−{W_{12}} dense coacervates are clearly distinct from many physically or covalently cross-linked polymeric networks that exhibit shear-thinning behaviors solely with increasing shear strain above a critical value due to dissociation or breakup of cross-linked network under large shear deformation. To the best of our knowledge, this is the first report of dense coacervates exhibiting strain-hardening behavior. Such strain-hardening behavior is highly similar to that observed in attractive colloidal gel, for which mode-coupling theory has been used to capture the dynamics of disordered colloidal systems related to particle localization.[71,74−76] We thereby attribute it to the clustering of $\{W_{12}\}$ in the aggregating complex particles as further examined by in situ SAXS characterization with shear.

To understand the structural change upon strain hardening in relation to proposed theoretical models such as non-Gaussian stretching and localized microstructure in the literature,[71,74−79] we employ SAXS characterization with in situ oscillatory shear under the same conditions as for nonlinear rheological measurements. The measured SAXS intensity profiles of PSBMA−$\{W_{12}\}$ dense coacervates at fixed $c_{e\{W12\}}/c_{SBMA}$ = 160% and c_{LiCl} = 0.3 M against varied γ are summarized in Figure 4b. At fixed ω = 6.28 rad/s and T = 30 °C, the $I(q)$ of PSBMA−$\{W_{12}\}$ dense coacervates at $q < 0.1$ Å^{-1} increases with increasing γ, in sharp contrast to strain-independent WAXS results at $q > 0.1$ Å^{-1} (inset of Figure 4b), suggesting that shear induces enlargement or increased number of PSBMA−$\{W_{12}\}$ complex particles. The microstructural change of complex particles is further scrutinized by the Kratky analysis, as shown in Figure 5a. At small γ = 10%, all of the Kratky plots of dense coacervates exhibit rising tails at $q > 0.1$ Å^{-1}, similar to the case without shear (see Figure 2a). At $\gamma > \gamma_c$ ∼50%, the tails in the Kratky plots are lowered with increasing γ, suggesting shear-enhanced packing of $\{W_{12}\}$ in complex particles. Again, using the GPA to verify the applicable q range of SAXS data for the Guinier analysis (see Supporting Figure S9), the γ-dependent R_g of complex particles is obtained by fitting the Guinier plots by eq 1. As clearly shown in Figure 5b, the R_g of complex particles increases monotonically with γ; for instance, R_g = 4.2 nm at γ = 10% is increased to 10.2 nm at γ = 700%. As the complex particles are considered as the cross-linking points for the critical-gel-like network structure of PSBMA−$\{W_{12}\}$ dense coacervates, the formation of denser and larger complex particles suggests enhanced physical cross-linking of the coacervate network by increased shear strain, which is structurally responsible for the observed strain-hardening behavior. As strain hardening is highly desired for smart functional materials working under extreme conditions, including self-healing body armors with high resistance to mechanical failure under impact and damping materials for absorbing shock waves from an earthquake or severe storms,[79−81] it could further broaden the application of POM-containing dense coacervates as new smart functional materials.

CONCLUSIONS

In summary, we have successfully revealed the microscopic structural organization of hybrid polyzwitterion−POM dense coacervates by SAXS combined with rheological characterization in response to varied compositions, temperature, and shear. Leveraging the strong X-ray scattering contrast of $\{W_{12}\}$, we describe the ultrastructures of critical-gel-like PSBMA−$\{W_{12}\}$ dense coacervates at nanometer scales by SAXS with in situ control of temperature and shear conditions. SAXS profiles strongly support the fractal structure of PSBMA−$\{W_{12}\}$ dense coacervates, which exhibits in the form of a critical-gel-like network as being cross-linked by complex particles consisting of PSBMA-linked $\{W_{12}\}$ aggregates. SAXS results show that the size of the complex particles grows with increasing $\{W_{12}\}$ to PSBMA ratio as well as decreasing salt concentration. Conversely, increasing temperature could result in smaller PSBMA−$\{W_{12}\}$ complex particles containing a reduced number of $\{W_{12}\}$ inside, which is consistent with the weakened viscoelasticity of dense coacervates with increased temperature. Distinct from most physically or covalently cross-linked polymeric networks that exhibit shear-thinning, PSBMA−$\{W_{12}\}$ dense coacervates exhibit intriguing strain hardening due to shear-enhanced packing of $\{W_{12}\}$ in the complex particles. To the best of our knowledge, it is for the first time that strain-hardening behavior is found in complex coacervate materials. In perspectives, with spontaneous and rapid two-aqueous-phase separating coacervation process, the strain-hardening and multiresponsive characteristics of such unconventional organic−inorganic macroion coacervates could lead to a new and facile paradigm of developing smart functional materials working under extreme environmental conditions.

ASSOCIATED CONTENT

Supporting Information

The Supporting Information is available free of charge at https://pubs.acs.org/doi/10.1021/acs.macromol.0c01618.

Additional experimental results of SAXS profiles after being normalized by transmission and background subtraction, Kratky plots, Guinier plots, Guinier peak analysis at varied composition, temperature, and shear (PDF)

AUTHOR INFORMATION

Corresponding Author

Yingxi Zhu − *Department of Chemical Engineering and Materials Science, Wayne State University, Detroit, Michigan 48202, United States;* orcid.org/0000-0002-7968-1640; Email: yzhu3@wayne.edu

Authors

Benxin Jing − *Department of Chemical Engineering and Materials Science, Wayne State University, Detroit, Michigan 48202, United States*

Manuela Ferreira − *Department of Chemical Engineering and Materials Science, Wayne State University, Detroit, Michigan 48202, United States;* orcid.org/0000-0001-8795-7179

Kehua Lin − *Department of Chemical Engineering and Materials Science, Wayne State University, Detroit, Michigan 48202, United States*

Ruipeng Li − *National Synchrotron Light Source II, Brookhaven National Laboratory, Upton, New York 11973, United States*

Benjamin M. Yavitt − *National Synchrotron Light Source II, Brookhaven National Laboratory, Upton, New York 11973, United States;* orcid.org/0000-0001-9308-7472

Jie Qiu − *School of Nuclear Science and Technology and State Key Laboratory of Multiphase Flow in Power Engineering, Xi'an Jiaotong University, Xi'an 710049, China;* orcid.org/0000-0001-7131-4881

Masafumi Fukuto − *National Synchrotron Light Source II, Brookhaven National Laboratory, Upton, New York 11973, United States*

Complete contact information is available at:

https://pubs.acs.org/10.1021/acs.macromol.0c01618

Notes

The authors declare no competing financial interest.

■ ACKNOWLEDGMENTS

The authors acknowledge the financial support from the National Science Foundation (NSF DMR-1743041) for this work. M.F. and K.L. are grateful for the financial support from NSF (CMMI-1914436) on the development of hybrid organic-inorganic functional materials and NSF (CMMI-1761418) on the characterization of POM-based complexes, respectively. This research used resources and the Complex Materials Scattering (CMS/11-BM) beamline of the National Synchrotron Light Source II, a U.S. Department of Energy (DOE) Office of Science User Facility operated for the DOE Office of Science by Brookhaven National Laboratory under Contract no. DE-SC0012704.

■ REFERENCES

(1) de Jong, H. G. B.; Kruyt, H. R. Coacervation (Partial miscibility on colloid systems) (Preliminary communication). *Proc. K. Akad. Wet. Amsterdam* **1929**, *32*, 849−856.

(2) Hyman, A. A.; Weber, C. A.; Jülicher, F. Liquid-Liquid Phase Separation in Biology. *Annu. Rev. Cell Dev. Biol.* **2014**, *30*, 39−58.

(3) Shin, Y.; Brangwynne, C. P. Liquid phase condensation in cell physiology and disease. *Science* **2017**, *357*, No. eaaf4382.

(4) Kizilay, E.; Kayitmazer, A. B.; Dubin, P. L. Complexation and Coacervation of Polyelectrolytes With Oppositely Charged Colloids. *Adv. Colloid Interface Sci.* **2011**, *167*, 24−37.

(5) Kayitmazer, A. B. Thermodynamics of Complex Coacervation. *Adv. Colloid Interface Sci.* **2017**, *239*, 169−177.

(6) Liu, X.; Chapel, J.-P.; Schatz, C. Structure, thermodynamic and kinetic signatures of a synthetic polyelectrolyte coacervating system. *Adv. Colloid Interface Sci.* **2017**, *239*, 178−186.

(7) Ali, S.; Prabhu, V. M. Characterization of the Ultralow Interfacial Tension in Liquid−Liquid Phase Separated Polyelectrolyte Complex Coacervates by the Deformed Drop Retraction Method. *Macromolecules* **2019**, *52*, 7495.

(8) Ruiter, L. D.; Jong, H. G. B. D. The interfacial tension af gum arabic-gelatin camplex-coacervates and their equilibrium liquids. *Proc. K. Ned. Akad. Wet., Ser. B* **1947**, *50*, 836−848.

(9) Jho, Y.; Yoo, H. Y.; Lin, Y.; Han, S.; Hwang, D. S. Molecular and structural basis of low interfacial energy of complex coacervates in water. *Adv. Colloid Interface Sci.* **2017**, *239*, 61−73.

(10) Lee, B. P.; Messersmith, P. B.; Israelachvili, J. N.; Waite, J. H. Mussel-Inspired Adhesives and Coatings. *Annual Review of Materials Research*; Clarke, D. R.; Fratzl, P., Eds., 2011; Vol. *41*, pp 99−132.

(11) Li, L.; Yan, B.; Yang, J. Q.; Chen, L. Y.; Zeng, H. B. Novel Mussel-Inspired Injectable Self-Healing Hydrogel with Anti-Biofouling Property. *Adv. Mater.* **2015**, *27*, 1294−1299.

(12) Voets, I. K.; de Keizer, A.; Cohen Stuart, M. A. Complex coacervate core micelles. *Adv. Colloid Interface Sci.* **2009**, *147−148*, 300−318.

(13) Blocher, W. C.; Perry, S. L. Complex coacervate-based materials for biomedicine. *Wiley Interdiscip. Rev.: Nanomed. Nanobiotechnol.* **2017**, *9*, No. e1442.

(14) Stewart, R. J.; Wang, C. S.; Shao, H. Complex Coacervates as A Foundation for Synthetic Underwater Adhesives. *Adv. Colloid Interface Sci.* **2011**, *167*, 85−93.

(15) Stewart, R. J.; Wang, C. S.; Song, I. T.; Jones, J. P. The role of coacervation and phase transitions in the sandcastle worm adhesive system. *Adv. Colloid Interface Sci.* **2017**, *239*, 88−96.

(16) Li, M.; Huang, X.; Tang, T. Y. D.; Mann, S. Synthetic cellularity based on non-lipid micro-compartments and protocell models. *Curr. Opin. Chem. Biol.* **2014**, *22*, 1−11.

(17) Spoelstra, W. K.; Deshpande, S.; Dekker, C. Tailoring the appearance: what will synthetic cells look like? *Curr. Opin. Biotechnol.* **2018**, *51*, 47−56.

(18) Douliez, J. P.; Perro, A.; Beven, L. Stabilization of All-in-Water Emulsions To Form Capsules as Artificial Cells. *Chembiochem* **2019**, *20*, 2546.

(19) Vieregg, J. R.; Tang, T. Y. D. Polynucleotides in cellular mimics: Coacervates and lipid vesicles. *Curr. Opin. Colloid Interface Sci.* **2016**, *26*, 50−57.

(20) Li, D.; Kelkar, M. S.; Wagner, N. J. Phase Behavior and Molecular Thermodynamics of Coacervation in Oppositely Charged Polyelectrolyte/Surfactant Systems: A Cationic Polymer JR 400 and Anionic Surfactant SDS Mixture. *Langmuir* **2012**, *28*, 10348−10362.

(21) Chollakup, R.; Beck, J. B.; Dirnberger, K.; Tirrell, M.; Eisenbach, C. D. Polyelectrolyte Molecular Weight and Salt Effects on the Phase Behavior and Coacervation of Aqueous Solutions of Poly(acrylic acid) Sodium Salt and Poly(allylamine) Hydrochloride. *Macromolecules* **2013**, *46*, 2376−2390.

(22) Chollakup, R.; Smitthipong, W.; Eisenbach, C. D.; Tirrell, M. Phase Behavior and Coacervation of Aqueous Poly(acrylic acid)−Poly(allylamine) Solutions. *Macromolecules* **2010**, *43*, 2518−2528.

(23) Li, L.; Srivastava, S.; Andreev, M.; Marciel, A. B.; de Pablo, J. J.; Tirrell, M. V. Phase Behavior and Salt Partitioning in Polyelectrolyte Complex Coacervates. *Macromolecules* **2018**, *51*, 2988−2995.

(24) Wang, J.; Cohen Stuart, M. A.; van der Gucht, J. Phase Diagram of Coacervate Complexes Containing Reversible Coordination Structures. *Macromolecules* **2012**, *45*, 8903−8909.

(25) Wang, X.; Li, Y.; Wang, Y.-W.; Lal, J.; Huang, Q. Microstructure of *β*-Lactoglobulin/Pectin Coacervates Studied by Small-Angle Neutron Scattering. *J. Phys. Chem. B* **2007**, *111*, 515−520.

(26) Le Ferrand, H.; Duchamp, M.; Gabryelczyk, B.; Cai, H.; Miserez, A. Time-Resolved Observations of Liquid−Liquid Phase Separation at the Nanoscale Using in Situ Liquid Transmission Electron Microscopy. *J. Am. Chem. Soc.* **2019**, *141*, 7202−7210.

(27) Kim, S.; Huang, J.; Lee, Y.; Dutta, S.; Yoo, H. Y.; Jung, Y. M.; Jho, Y.; Zeng, H.; Hwang, D. S. Complexation and Coacervation of Like-charged Polyelectrolytes Inspired by Mussels. *Proc. Natl. Acad. Sci. USA* **2016**, *113*, E847−E853.

(28) Sing, C. E.; Perry, S. L. Recent progress in the science of complex coacervation. *Soft Matter* **2020**, *16*, 2885−2914.

(29) Uversky, V. N. Protein intrinsic disorder-based liquid−liquid phase transitions in biological systems: Complex coacervates and membrane-less organelles. *Adv. Colloid Interface Sci.* **2017**, *239*, 97−114.

(30) Cooper, C. L.; Dubin, P. L.; Kayitmazer, A. B.; Turksen, S. Polyelectrolyte−protein Complexes. *Curr. Opin. Colloid Interface Sci.* **2005**, *10*, 52−78.

(31) Cousin, F.; Gummel, J.; Combet, S.; Boué, F. The model Lysozyme−PSSNa system for electrostatic complexation: Similarities and differences with complex coacervation. *Adv. Colloid Interface Sci.* **2011**, *167*, 71−84.

(32) Miyake, M. Recent progress of the characterization of oppositely charged polymer/surfactant complex in dilution deposition system. *Adv. Colloid Interface Sci.* **2017**, *239*, 146−157.

(33) Zhao, W.; Wang, Y. Coacervation with surfactants: From single-chain surfactants to gemini surfactants. *Adv. Colloid Interface Sci.* **2017**, *239*, 199−212.

(34) Leisner, D.; Imae, T. Interpolyelectrolyte Complex and Coacervate Formation of Poly(glutamic acid) with a Dendrimer Studied by Light Scattering and SAXS. *J. Phys. Chem. B* **2003**, *107*, 8078−8087.

(35) Valley, B.; Jing, B.; Ferreira, M.; Zhu, Y. Rapid and Efficient Coacervate Extraction of Cationic Industrial Dyes from Wastewater. *ACS Appl. Mater. Interfaces* **2019**, *11*, 7472−7478.

(36) Jing, B.; Ferreira, M.; Gao, Y.; Wood, C.; Li, R.; Fukuto, M.; Liu, T.; Zhu, Y. Unconventional Complex Coacervation between Neutral Polymer and Inorganic Polyoxometalate in Aqueous Solution via Direct Water Mediation. *Macromolecules* **2019**, *52*, 8275.

(37) Jing, B.; Xu, D.; Wang, X.; Zhu, Y. Multiresponsive, Critical Gel Behaviors of Polyzwitterion−Polyoxometalate Coacervate Complexes. *Macromolecules* **2018**, *51*, 9405−9411.

(38) Jing, B.; Qiu, J.; Zhu, Y. Organic-inorganic macroion coacervate complexation. *Soft Matter* **2017**, *13*, 4881−4889.

(39) Carn, F.; Steunou, N.; Djabourov, M.; Coradin, T.; Ribot, F.; Livage, J. First Example of Biopolymer-polyoxometalate Complex Coacervation in Gelatin-decavanadate Mixtures. *Soft Matter* **2008**, *4*, 735−738.

(40) Singh, S. S.; Aswal, V. K.; Bohidar, H. B. Structural Studies of Agar−gelatin Complex Coacervates by Small Angle Neutron Scattering, Rheology and Differential Scanning Calorimetry. *Int. J. Biol. Macromol.* **2007**, *41*, 301−307.

(41) Krogstad, D. V.; Choi, S.-H.; Lynd, N. A.; Audus, D. J.; Perry, S. L.; Gopez, J. D.; Hawker, C. J.; Kramer, E. J.; Tirrell, M. V. Small Angle Neutron Scattering Study of Complex Coacervate Micelles and Hydrogels Formed from Ionic Diblock and Triblock Copolymers. *J. Phys. Chem. B* **2014**, *118*, 13011−13018.

(42) Kizilay, E.; Seeman, D.; Yan, Y.; Du, X.; Dubin, P. L.; Donato-Capel, L.; Bovetto, L.; Schmitt, C. Structure of Bovine [small beta]-Lactoglobulin-lactoferrin Coacervates. *Soft Matter* **2014**, *10*, 7262−7268.

(43) Fares, H. M.; Ghoussoub, Y. E.; Delgado, J. D.; Fu, J.; Urban, V. S.; Schlenoff, J. B. Scattering Neutrons along the Polyelectrolyte Complex/Coacervate Continuum. *Macromolecules* **2018**, *51*, 4945−4955.

(44) Spruijt, E.; Leermakers, F. A. M.; Fokkink, R.; Schweins, R.; van Well, A. A.; Cohen Stuart, M. A.; van der Gucht, J. Structure and Dynamics of Polyelectrolyte Complex Coacervates Studied by Scattering of Neutrons, X-rays, and Light. *Macromolecules* **2013**, *46*, 4596−4605.

(45) Hwang, D. S.; Zeng, H.; Srivastava, A.; Krogstad, D. V.; Tirrell, M.; Israelachviliab, J. N.; Waite, J. H. Viscosity and Interfacial Properties in A Mussel-inspired Adhesive Coacervate. *Soft Matter* **2010**, *6*, 3232−3236.

(46) Huang, K.-Y.; Yoo, H. Y.; Jho, Y.; Han, S.; Hwang, D. S. Bicontinuous Fluid Structure with Low Cohesive Energy: Molecular Basis for Exceptionally Low Interfacial Tension of Complex Coacervate Fluids. *ACS Nano* **2016**, *10*, 5051−5062.

(47) Kizilay, E.; Dinsmore, A. D.; Hoagland, D. A.; Sun, L.; Dubin, P. L. Evolution of hierarchical structures in polyelectrolyte−micelle coacervates. *Soft Matter* **2013**, *9*, 7320−7332.

(48) Marciel, A. B.; Srivastava, S.; Tirrell, M. V. Structure and rheology of polyelectrolyte complex coacervates. *Soft Matter* **2018**, *14*, 2454−2464.

(49) Neumann, R. Polyoxometalate complexes in organic oxidation chemistry. *Prog. Inorg. Chem.* **1998**, *47*, 317−370.

(50) Hill, C. L.; C. M. P.-M. Homogeneous catalysis by transition metal oxygen anion clusters. *Coord. Chem. Rev.* **1995**, *143*, 407−455.

(51) Lehmann, J.; A. G.-A; Coronado, E.; Loss, D. Spin qubits with electrically gated polyoxometalate molecules. *Nat. Nanotechnol.* **2007**, *2*, 312−317.

(52) Rhule, J. T.; C. L. H; Judd, D. A.; Schinazi, R. F. Polyoxometalates in medicine. *Chem. Rev.* **1998**, *98*, 327−358.

(53) Hill, C. L.; M. S. W; Schinazi, R. F. Anti-HIV-1 activity, toxicity, and stability studies of representative structural families of polyoxometalates. *J. Med. Chem.* **1990**, *33*, 2767−2772.

(54) Jing, B.; Qiu, J.; Zhu, Y. Organic−inorganic macroion coacervate complexation. *Soft Matter* **2017**, *13*, 4881−4889.

(55) Mary, P.; Bendejacq, D. D.; Labeau, M.-P.; Dupuis, P. Reconciling Low- and High-Salt Solution Behavior of Sulfobetaine Polyzwitterions. *J. Phys. Chem. B* **2007**, *111*, 7767−7777.

(56) Delgado, J. D.; Schlenoff, J. B. Static and Dynamic Solution Behavior of a Polyzwitterion Using a Hofmeister Salt Series. *Macromolecules* **2017**, *50*, 4454−4464.

(57) Wang, F.; Yang, J.; Zhao, J. Understanding Anti-polyelectrolyte Behavior of a Well-defined Polyzwitterion at the Single-chain Level. *Polym. Int.* **2015**, *64*, 999−1005.

(58) Liu, Y.; Winter, H. H.; Perry, S. L. Linear viscoelasticity of complex coacervates. *Adv. Colloid Interface Sci.* **2017**, *239*, 46−60.

(59) Scattering Length Density. http://gisaxs.com/index.php/Scattering_Length_Density.

(60) Winter, H. H., The Critical Gel. In *Structure and Dynamics of Polymer and Colloidal Systems*; Borsali, R.; Pecora, R., Eds.; Springer: Dordrecht, Netherlands, 2002; pp 439−470.

(61) Rubinstein, M.; Colby, R. H. *Polymer Physics*; Oxford University Press, 2003.

(62) Muthukumar, M. Screening effect on viscoelasticity near the gel point. *Macromolecules* **1989**, *22*, 4656−4658.

(63) Buchecker, T.; Le Goff, X.; Naskar, B.; Pfitzner, A.; Diat, O.; Bauduin, P. Polyoxometalate/Polyethylene Glycol Interactions in Water: From Nanoassemblies in Water to Crystal Formation by Electrostatic Screening. *Chem. − Eur. J.* **2017**, *23*, 8434−8442.

(64) Mertens, H. D. T.; Svergun, D. I. Structural characterization of proteins and complexes using small-angle X-ray solution scattering. *J. Struct. Biol.* **2010**, *172*, 128−141.

(65) Rambo, R. P.; Tainer, J. A. Characterizing flexible and intrinsically unstructured biological macromolecules by SAS using the Porod-Debye law. *Biopolymers* **2011**, *95*, 559−571.

(66) Smirnov, A. V.; Deryabin, I. N.; Fedorov, B. A. Small-angle scattering: the Guinier technique underestimates the size of hard globular particles due to the structure-factor effect. *J. Appl. Crystallogr.* **2015**, *48*, 1089−1093.

(67) Putnam, C. D. Guinier peak analysis for visual and automated inspection of small-angle X-ray scattering data. *J. Appl. Crystallogr.* **2016**, *49*, 1412−1419.

(68) André Guinier, G. F. *Small-Angle Scattering of X-rays*; John Wiley and Sons: New York, 1955.

(69) Ferry, J. D. *Viscoelastic Properties of Polymers*, 3rd ed.; John Wiley: New York, 1980.

(70) Adhikari, S.; Prabhu, V. M.; Muthukumar, M. Lower Critical Solution Temperature Behavior in Polyelectrolyte Complex Coacervates. *Macromolecules* **2019**, *52*, 6998−7004.

(71) Gisler, T.; Ball, R. C.; Weitz, D. A. Strain Hardening of Fractal Colloidal Gels. *Phys. Rev. Lett.* **1999**, *82*, 1064−1067.

(72) Kraus, G. Mechanical losses in carbon-black-filled rubbers. *J. Appl. Polym. Sci.: Appl. Polym. Symp.* **1984**, 75−92.

(73) Huber, G. On the Mechanism of Hydrodynamic Reinforcement in Elastic Composites. *Macromolecules* **2002**, *35*, 9204−9210.

(74) Hsiao, L. C.; Kang, H.; Ahn, K. H.; Solomon, M. J. Role of shear-induced dynamical heterogeneity in the nonlinear rheology of colloidal gels. *Soft Matter* **2014**, *10*, 9254−9259.

(75) Bergenholtz, J.; Fuchs, M. Nonergodicity transitions in colloidal suspensions with attractive interactions. *Phys. Rev. E* **1999**, *59*, 5706−5715.

(76) Chen, Y.-L.; Schweizer, K. S. Microscopic theory of gelation and elasticity in polymer−particle suspensions. *J. Chem. Phys.* **2004**, *120*, 7212−7222.

(77) Brown, E.; Jaeger, H. M. Shear thickening in concentrated suspensions: phenomenology, mechanisms and relations to jamming. *Rep. Prog. Phys.* **2014**, *77*, No. 046602.

(78) van Egmond, J. W. Shear-thickening in suspensions, associating polymers, worm-like micelles, and poor polymer solutions. *Curr. Opin. Colloid Interface Sci.* **1998**, *3*, 385−390.

(79) Gürgen, S.; Kuşhan, M. C.; Li, W. Shear thickening fluids in protective applications: A review. *Prog. Polym. Sci.* **2017**, *75*, 48−72.

(80) Wagner, N. J.; Brady, J. F. Shear thickening in colloidal dispersions. *Phys. Today* **2009**, *62*, 27−32.

(81) Wool, R. P. Self-healing materials: a review. *Soft Matter* **2008**, *4*, 400−418.